



RESEARCH ARTICLE - MECHANICAL ENGINEERING

Numerical Investigation of the Thermosiphon-Thermoelectric Generator by Different Parameters

Mortatha Faleh Majed¹, Mahdi Moghimi^{1*}

¹Department of Energy Conversion, Mechanical Engineering College, Iran University of Science and Technology (IUST), Tehran, Islamic Republic of Iran

* Corresponding author E-mail: moghimi@iust.ac.ir

Article Info.	Abstract
<i>Article history:</i> Received 15 January 2025 Accepted 01 June 2025 Publishing 30 June 2025	<p>This paper aims to enhance the performance of thermoelectric generators (TEGs) in converting waste heat into electrical energy by employing nanofluids. The research addresses the limitations of traditional working fluids like water, which have low thermal conductivity, and explores the use of nanofluids in a thermosiphon system integrated with a TEG. The CFD tool used in this work is ANSYS Fluent R23 for solving the problem, and the turbulent flow is modeled using the SST $k-\omega$ model. The second-order upwind discretization scheme is used for solving the energy, continuity, and momentum equations. The study starts with analyzing heat sink geometry, focusing on fin height and spacing. Simulations demonstrate that reducing fin spacing from 5.50 mm to 2.50 mm, despite 70% reduction in the fins' number, optimizes performance by increasing the wetted surface area, thereby lowering heat sink temperatures. Similarly, increasing fin height to an optimal range of 5–25 mm improves heat dissipation, even though it reduces the local convection heat transfer coefficient, highlighting the importance of surface area in passive cooling systems. The study also explores the cooling potential of Al_2O_3 and CuO water nanofluids at a 4% concentration. Al_2O_3-water reduces the heat sink temperature by 17%, while CuO-water achieves a 13% reduction. Further increases in nanoparticle concentration enhance the cooling performance, with an additional temperature drop of approximately 8°C observed. Under extreme conditions with a heat flux of 75,000 W/m², the optimized heat sink design maintained a cold-side temperature of 39 °C when cooled by the Nano fluid. The simulations visually confirm the system's effectiveness, demonstrating how geometric optimization and advanced materials work together to enhance TEG performance. This investigation offers valuable insights for improving energy conversion technologies, particularly in waste heat recovery.</p>

This is an open-access article under the CC BY 4.0 license (<http://creativecommons.org/licenses/by/4.0/>)

Publisher: Middle Technical University

Keywords: Thermo Siphon System; Thermoelectric Generator; Nanofluid; Thermal Energy; Heat Sink.

1. Introduction

Numerically, the effects of nanofluids on the thermal energy performance of a thermosiphon heat transporting system coupled with a thermoelectric generator (TEG) are explored, and major increases in the efficiency of heat transfer and energy conversion are obtained. Nanofluids are fluids consisting of suspended nanoparticles, and their application is to increase the heat transfer capabilities of thermosiphon systems, which are heat transfer systems that rely on a phase change process to efficiently transfer heat [1]. Nanofluid integration in thermosiphon systems can improve heat transfer efficiency, which will be important to enhance the TEGs' performance, which requires a temperature differential to leverage Seebeck's effect to generate electricity [2, 3]. The use of Nano fluids like Al_2O_3 , TiO_2 , and graphene increases the cooling performance of TEG systems leading to enhanced output power and conversion efficiency [4-6]. For instance, we demonstrate that TEGs operated with Al_2O_3 nanofluids have a 70% increase in maximum power output and a 45% increase with SiO_2 nanofluids [2]. In addition, it is demonstrated that Nano fluids made using TiO_2 can improve TEG performance by 17% than distilled water, providing a better cooling alternative [5]. Further improvement can be seen in the segmentation of thermoelectric legs, especially for a 2n-1p configuration, and hollow leg structures show better performance than filled ones [5]. Furthermore, Nano fluids can enhance the heat collection and cooling process, as shown by the emergence of Nano fluidic thermosiphon heat sinks that have exhibited enhancements in cooling capacity and performance at proper nanoparticle concentrations [7, 8]. Since then, it has been shown that Nano fluids also can be integrated into the TEG systems for WHR applications, which can contribute greatly to improving the heat transfer process and raise their efficiency [3]. Also, in solar thermoelectricity generating systems, the use of nano-fluid simplifies heat exchange, reduces thermal energy loss, and increases the net system efficiency [6]. These findings have been further validated with numerical models and simulations, for example, using ANSYS Workbench, which have shown that nanofluids could dramatically increase the performance of the TEG system [5]. For instance, graphene nanoplatelet aqueous nanofluids have shown increases of 26.39% in output power, and 14.74% in conversion efficiency of TEG systems [6].

The potential of Nano fluids to revolutionize the design and operation of thermosiphon systems and TEGs is thus established, providing a basis for more efficient and sustainable energy solutions. But more work, in both the operational and material development areas, will be needed before these systems can achieve full-scale commercialization[3]. Through numerical investigation, Nano fluids show promising ability in

Nomenclature & Symbols			
TEG	Thermoelectric Generator	SDD	Simulation-Driven Design
WHR	Waste Heat Recovery	PCM	Phase Change Material
HTPF	Hydro-Thermal Performance Factor	A_{abs}	Area of the Absorber Plane (m^2)
CFD	Computational Fluid Dynamics	ρ	Density of fluid (kg/m^3)

enhancing the thermal energy efficiency of TEGs coupling systems, contributing to more effective energy conversion and utilization. As well, through numerical investigations of different fin configurations in thermoelectric generator (TEG) interacting heat sinks, significant input into optimizing thermal energy performance in thermosiphon systems can be gained. Effects of fin shapes, arrangements and materials on the efficiency and power output of TEG systems have been studied in many studies. For example, application of inclined and combined fins in heat exchangers has resulted in 29% and 35% increase in net power output and overall efficiency, respectively, over straight fins without exceeding the maximum allowable stress limit [9]. Twisted fins with diamond-shaped perforations at a twisting angle of 540° can provide a 25% enhancement in the hydrothermal performance factor (HTPF) and a 46% increase in the Nusselt number, similar to the results reported in [10]. Shark scale-based fins in microchannel cooling systems also demonstrate improved heat transfer rates and reduced friction losses, particularly when using nanofluids like graphene oxide and silver, which result in a performance criterion larger than one [11]. Curved fins have been discovered in thermal power generation systems used to recover waste heat in ships, where these fins contribute to the creation of tip leakage vortices. This enhances the efficiency of power generation and heat transfer compared to straight fins [12]. In high-concentrated solar cells, sinusoidal fins in micro-channel heat sinks can significantly improve electrical performance, with efficiency gains observed by increasing the number of fins and adjusting the sine wave's amplitude and wavelength [13]. Sickle fins integrated into the polygonal heat exchangers in TEG systems improve power output and temperature uniformity, although higher pressure drop may occur [14]. Studies have shown that pin fins, especially in staggered configurations, enhance the thermal-hydraulic coefficient of performance and power generation capacity, with thicker fins resulting in higher power output [15]. Specifically designed cooling fins, such as 17-pin fins, can contribute to enhanced thermal efficiency and improved performance in power cable surface waste heat recovery applications [16]. Finally, increasing the fins' number in the heat sink can contribute to lowering the junction temperature and increasing heat dissipation. However, having too many fins may degrade the thermal benefit [17]. This set of studies collectively demonstrates the vital role fin configuration plays in improving thermal energy performance of TEG – thermosiphon systems, further emphasizing the need for fin design that represents the best efficiency and power output under different system conditions.

This study examines the effects of nanofluids on the characteristics of the thermal cell system and the performance of thermal energy for thermal energy conversion units (TEG) through numerical methods. The main challenge in this regard is to improve the efficiency of heat transfer in thermosiphon systems to achieve better performance in TEG units. Previous research has shown that nanofluid technology has great potential to increase cooling and energy production capacity in TEG systems. However, more research is needed to better understand the capabilities of these fluids in enhancing the process of transforming energy and increasing the efficiency of the system.

2. Materials and Methodology

We utilized ANSYS Fluent R23 for the simulations, leveraging its licensed computational fluid dynamics (CFD) capabilities. A pressure-based solver was employed to model fluid flow and heat transfer under steady-state conditions. To accurately capture turbulence effects, we implemented the k- ω SST (Shear Stress Transport) model, known for its effectiveness in predicting adverse pressure gradients and separated flows. The governing equations for mass, momentum, and energy transfer were solved using a second-order accurate upwind scheme to enhance solution precision. The SIMPLE (Semi-Implicit Method for Pressure Linked Equations) algorithm was employed for pressure-velocity coupling. Convergence was monitored by tracking the residuals of the governing equations, with a convergence criterion set to $1e-6$ for all residuals. (Fig. 1) presents the Flowchart of the CFD simulation.

2.1. Geometric modelling and computational domain

Ansys Fluent was used to simulate the combined fluid flow and heat transfer. A wide range of parameters were investigated using the numerical formulation, validated successfully with experimental results. This capability facilitates the heat dissipation system's simulation-driven design. Within the geometry, various spacings of fins and heights were numerically examined to optimize for minimal thermal resistance and understand their impact on overall heat transfer. The 3D computational domain includes the tank volume, the inner wall of the pipe, multiple outer walls, the heater mass, and the fluid-free surface, without modeling the thickness of the tank and pipe walls. A specific heat flux is applied to an area of 40 mm x 40 mm in the aluminum heat sink base to simulate the thermal signature of a TEG. The model simulates the fluid inside the heat sink, as well as the feed and return lines, tank, and manifold. Since the manifold housing is thermally connected to the hot bed, it contributes to the transfer of heat to the confined fluid, which is considered a transfer effect. To simplify the model and reduce solution times, symmetry is applied whenever possible. (Fig. 2) shows the model simulation with the main dimensions.

2.2. Mesh generation

A meticulously designed mesh is a cornerstone of accurate and reliable computational fluid dynamics (CFD) simulations. In this paper, the meshing process was discretized in the selected TEG system, ensuring that it captures the intricate fluid dynamics and heat transfer phenomena under investigation. After a rigorous grid independence test, the mesh was structured and fine-tuned to strike a balance between computational efficiency and resolution.

The meshing strategy adopted in this study employs a structured Polyhedral mesh approach to represent the radiator geometry effectively (Fig. 3). Structured meshes consist of well-organized cells or elements that align with the geometry's contours and boundaries, enhancing the accuracy of flow and heat transfer predictions.

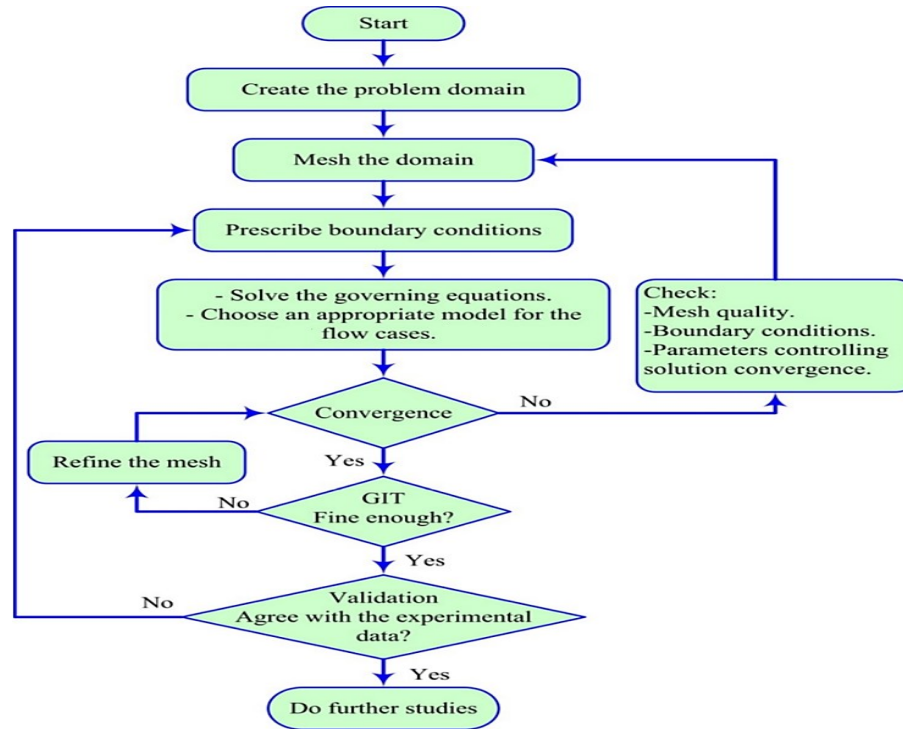


Fig. 1. Flowchart of CFD simulation

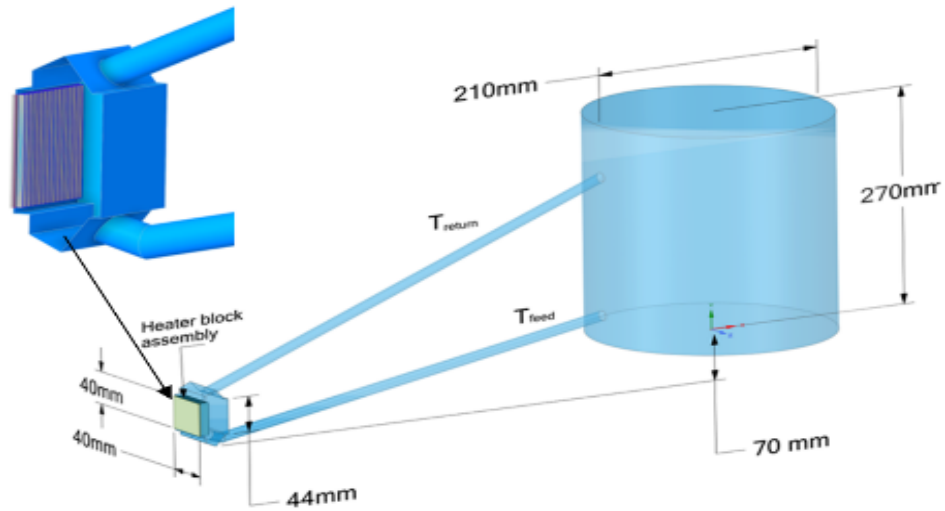


Fig. 2. Diagram of the numerical domain

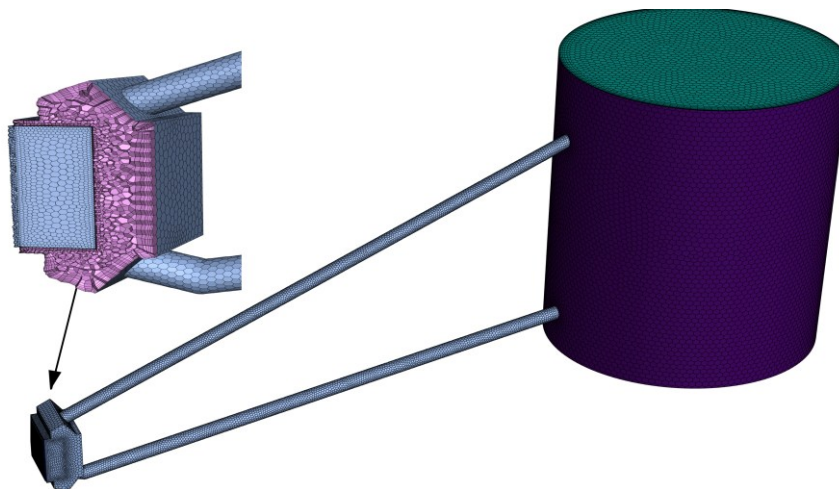


Fig. 3. Polyhedral mesh for TEG system

2.2.1. Mesh element size and grid independence test and validation

One of the critical aspects of numerical simulations is ensuring that the obtained outcomes are independent of the discretization level or grid resolution. The precision and accuracy of numerical findings are often proportional to the mesh size, with finer grids typically yielding more accurate solutions, albeit at a higher computational cost. To strike a balance between computational efficiency and solution accuracy, it is essential to perform a grid independence study.

In the present research, a grid independence study was conducted to determine the appropriate element size for the numerical simulations. Five distinct element numbers were selected for this purpose: 250638, 504525, 845260, 948925, 1083256, and 1462638 elements. The objective was to assess the variation in the computed results, specifically the heat transfer coefficient distribution over the heat sink, as the grid resolution was increased.

The results of the grid independence study are presented in Table 1. This table depicts the heat transfer coefficient distribution over the heat sink for the different grid resolutions considered. By analyzing the data, it was observed that the relative percentage error between the results obtained with 1083256 and 1462638 elements was only 0.88%. Such a small discrepancy is typically considered negligible in numerical simulations, indicating that further mesh refinement would not yield significantly different results.

Consequently, based on the grid independence study, a grid size of 1083256 elements was deemed appropriate for the present research. This choice strikes a balance between computational efficiency and numerical accuracy, as the solutions obtained with this mesh size can be considered grid-independent, or independent of the discretization level. By establishing grid independence, confidence in the numerical findings is enhanced, and the simulations can proceed with the assurance that the results are not unduly influenced by the mesh resolution.

Table 1. Variation in average Nusselt number as a function of mesh size

Elements number	h_{avr}	Relative error
250638	385.236
504525	408.235	5.63 %
845260	420.235	2.85 %
948925	431.235	2.55 %
1083256	442.2402	2.48 %
1462638	446.2056	0.88 %

The presented system is verified by comparing its outcomes with the numerical data from Chen et al [18]. The TEG is evaluated under identical operating conditions, where the temperature is kept constant at 303 K on the cold side and varied from 340 K to 430 K on the hot side. All input data, parameters, and configurations are kept the same as in the Chen et al. model [18].

Fig. 3 compares the results of the current model with Chen et al [18]. Numerical findings for the TEG's output power as a function of the hot side's temperature, as shown in Fig. 4, demonstrate good agreement between the current scheme's outcomes and the numerical results presented by Chen et al [18]. This suggests that the designed system offers a solution with a high precision, reliability in computations, and more effective handling of electrical and thermal field parameters compared to the previous study.

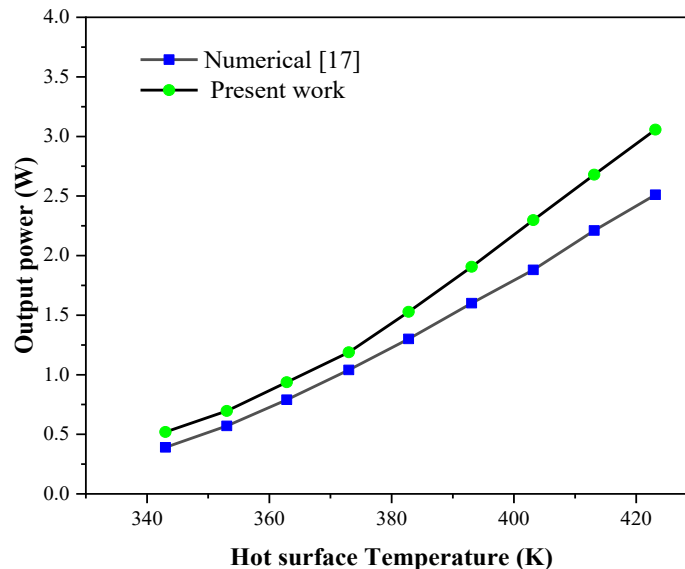


Fig. 4. The developed TEG system's output power compared with the results of Chen et al.[18]

2.3. Assumptions and boundary conditions

In a passive liquid cooling system's simulation-driven design for a TEG, several key assumptions and boundary conditions are made to facilitate accurate modeling of thermal and fluid dynamics. The simulations assume steady-state conditions, with constant temperatures and heat flows over time. The thermal properties of materials, such as density, specific heat, and thermal conductivity, are considered constant and do not vary with temperature, while radiative heat transfer is deemed negligible compared to conductive and convective heat transfer. The flow within the thermosiphon is assumed to be laminar, simplifying fluid dynamics calculations, and the generated heat by the TEG is assumed to be steadily distributed across its surface. The resistance of thermal contact between the TEG and the heat sink, as well as between other contacting surfaces,

is considered negligible. The convective heat transfer coefficient is assigned to surfaces that are exposed to airstream or fluid, and boundary conditions specify the temperature of the hot side, cold side, and ambient. For surfaces where heat transfer is negligible, adiabatic boundaries are employed. Coolant circulation is the result of proper inlet and outlet conditions with the pressure drop and flow rate adjusted for natural convection and is subjected to the no-slip condition at solid-fluid interfaces. Modeling of their behavior is simplified by assuming that nanofluid properties are homogeneous and isotropic. Setting up finite element or computational fluid dynamics (CFD) models involves many assumptions and boundary conditions essential for simplifying the problem so that it achieves sufficient accuracy. The results are validated against experimental data to verify that the assumptions and boundary conditions are effective for real world applications.

2.4. Governing equations

The governing equations for a passive natural heat transfer thermosiphon in transient flow involve the conservation of mass, momentum, and energy. These equations describe how the fluid moves and how heat is transferred within the thermosiphon over time. The equations can be expressed as follows:

- Conservation of Mass (Continuity Equation)

The continuity equation ensures that mass is conserved within the thermosiphon system. It can be written as:

$$\frac{\partial \rho}{\partial t} + \nabla \cdot (\rho V) = 0 \quad (1)$$

In above equation, v , t , and ρ represent the velocity vector, time, and fluid density.

- Conservation of Momentum (Navier-Stokes Equation)

The momentum equation describes the forces acting on the fluid. Natural convection in a thermosiphon can be simplified under the Boussinesq approximation, assuming density variations are significant only in the buoyancy term. The equation is:

$$\rho \left(\frac{\partial v}{\partial t} + (v \cdot \nabla)v \right) = -\nabla p + \mu \nabla^2 v + \rho g \beta (T - T_0) \quad (2)$$

In above equation: μ and p denote to the dynamic viscosity and pressure; T and T_0 are the local and reference temperature, respectively; and g and β represent the gravitational acceleration vector and thermal expansion coefficient.

- Conservation of Energy

The energy equation describes the temperature distribution within the fluid. It is given by:

$$\rho C_p \left(\frac{\partial T}{\partial t} + V \cdot \nabla T \right) = K \nabla^2 T \quad (3)$$

In this statement: K and C_p are the thermal conductivity and the specific heat capacity, respectively.

2.5. Thermophysical properties of nano fluid

The single-phase approach makes simplifying assumptions by treating the nanofluid as a homogeneous mixture with uniform properties, while there may be non-uniformity, particle clustering, slip velocity between phases, and effects like sedimentation and thermophoresis that are not accounted for. It uses approximate empirical correlations to estimate the thermophysical properties like viscosity and thermal conductivity, whereas the actual values depend on factors like particle shape, interactions, and concentration. These limitations of assuming a homogeneous single-phase mean the model may not reliably predict the true nanofluid behavior, especially at higher particle loadings. The numerical results can deviate from experimental values due to the approximate nature of the single-phase assumptions. More complex discrete phase models may be needed for accuracy by explicitly accounting for the solid nanoparticles and their interactions.

As mentioned previously, some experimental results have helped characterize nanofluid properties by using classical models derived from single-phase mixtures. The subsequent equations can be utilized to calculate the Nano fluids' density and specific heat capacity [19-22].

$$\rho_{nf} = \phi_p \rho_p + (1 - \phi_p) \rho_{bf} \quad (4)$$

Equation 3 first employs the specific heat [19-28].

$$C_{nf} = \frac{\phi_p \rho_p C_p + (1 - \phi_p) \rho_{bf} C_{bf}}{\rho_{nf}} \quad (5)$$

As previously stated, it is worth noting that classical models may not yield the same level of advantages and efficacy as experimental data. In this study, the thermal conductivity and viscosity values reported by [29, 30]. It was used to obtain the most accurate numerical results for both nanofluids and hybrid nanofluids at various volumetric concentrations.

Thermal conductivity of nanofluid:

$$\frac{k_{nf}}{k_{bf}} = 1 + 4.4 Re^{0.4} Pr^{0.66} \left(\frac{T}{T_{fr}} \right)^{10} \left(\frac{k_p}{k_{bf}} \right)^{0.03} \phi^{0.66} \quad (6)$$

The Reynolds number of nanoparticles is expressed as:

$$Re = \frac{\rho_{bf} u_B d_p}{\mu_{bf}} \quad (7)$$

The nanoparticle Brownian velocity u_B is determined by:

$$u_B = \frac{2k_{bf} T}{\pi \mu_{bf} d_p^2} \quad (8)$$

The Corcione model [29] was used with high accuracy in this work to measure the viscosity of nanofluids and hybrid nanofluids.

$$\mu_{nf} = \left[\frac{1}{1 - 34.87 \left(\frac{d_p}{d_{bf}} \right)^{-0.3} \phi_p^{1.03}} \right] \mu_{bf} \quad (9)$$

$$d_{bf} = 0.1 \left(\frac{6M}{N\pi\rho_{bf}} \right)^{0.33} \quad (10)$$

In the above equation:

M: Molecular weight of water, M (kg/mol) = 1.80E-02.

N: Avogadro number, N (mol⁻¹) = 6.02E+23.

2.6. Coupled heat transfer and thermoelectric equations for TEG simulation

The equations used to simulate the Thermoelectric Generator (TEG) in ANSYS Fluent involve coupling the heat transfer equations with the thermoelectric effects. The key equations involved in the simulation are:

2.6.1. Heat Transfer Equations

- Conduction: Fourier's Law of Heat Conduction

This law describes the heat transfer by conduction, and it is given by:

$$q = -k \nabla T \quad (11)$$

In the above equation, ∇T , k , and q are the temperature gradient, thermal conductivity (W/m·K), and heat flux (W/m²), respectively.

- Convection: Newton's Law of Cooling

This law describes the heat transfer by convection, and it is given by:

$$q = h(T_s - T_\infty) \quad (12)$$

In this equation, T_s and T_∞ are the surface and fluid temperature sufficiently far from the surface, while q and h represent the heat flux (W/m²) and convective heat transfer coefficient (W/m²·K), respectively.

2.6.2. Thermoelectric Effects

2.6.2.1. Seebeck Effect: The generation of an electrical potential (EMF) as a result of a temperature gradient across a thermoelectric material.

2.6.2.2. Peltier Effect: The absorption or release of heat at the junction of two different conductors as a result of the flow of an electric current through the junction.

2.6.2.3. Thomson Effect: The absorption or release of heat as a result of the flow of electric current through a conductor in which there is a temperature gradient.

The equations governing thermal effects can be expressed as follows:

- Seebeck Effect:

$$V = \alpha * \Delta T \quad (13)$$

In this equation, V is the Seebeck voltage (or EMF), α is the Seebeck coefficient (or thermoelectric power), and ΔT is the temperature difference across the thermoelectric material.

- Peltier Effect:

$$Q = \pi * I \quad (14)$$

In this equation, Q is the rate of heat absorption or release, I is the electric current, and π is the Peltier coefficient.

- Thomson Effect:

$$Q = \beta * I * \frac{dT}{dx} \quad (15)$$

In this equation, Q , β , dT/dx , and I represent the rate of heat absorption or release, Thomson coefficient, temperature gradient along the conductor, and electric current, respectively.

In ANSYS Fluent, these equations are coupled with the heat transfer equations and solved iteratively to simulate the thermoelectric generator's performance. The simulation also accounts for the thermoelectric materials' properties, such as thermal and electrical conductivity, and thermoelectric properties (Seebeck coefficient, Peltier coefficient, and Thomson coefficient).

Additionally, ANSYS Fluent may incorporate other relevant equations and models, such as fluid flow equations (if applicable), electrical circuit equations, and models for energy conversion and heat transfer between different components of the TEG system.

It's important to note that the specific implementation and coupling of these equations in ANSYS Fluent may vary depending on the version and the specific settings and models used for the simulation.

3. Results and Discussion

The main objective of this research was to develop a straightforward but effective thermal hardware-based solution to the TEG cooling systems' typical problems with parasitic power draw and long-term reliability. In this research, the system is optimized in a Simulation Driven Design

(SDD) manner using computational fluid dynamics (CFD) simulations first by investigating the optimal geometric parameters of the heat sink and next using nanofluids to enhance the heat transfer performance. It then computes the performance of various nanofluids as potential replacements for the cooling system with water. Engineered colloidal suspensions of nanoparticles in a base fluid, called nanofluids, have been shown to enhance heat transfer properties. The effect of the use of different nanoparticle materials and different concentrations on the thermal conductivity and convective heat transfer coefficient are investigated by means of simulations. To better understand the effects of concentration on thermal performance, multiple types of nanofluids were studied at various concentrations for which they demonstrated the best thermal performance.

3.1. Effect of fin spacing on the heat transfer coefficient

Research on the effect of fin spacing on heat transfer performance in the passive liquid cooling system of thermoelectric generators (TEGs) reveals an interesting interplay between competing thermal and hydraulic phenomena. This study, which is part of a broader simulation-driven design (SDD) approach, provides important insights into improving heat sink design in low-flow natural convection systems.

Four different fin spacings were investigated: 2.50 mm, 3.50 mm, 4.50 mm, and 5.50 mm. As the fin spacing increased, the number of fins within the fixed 40 mm × 40 mm footprint decreased from 17 to 13, 8, and finally 5 fins. This reduction in fin count is a direct consequence of maintaining a constant fin thickness while increasing the spacing, highlighting the inherent trade-off between fin density and inter-fin gap.

Computational fluid dynamics (CFD) simulations revealed that as the spacing of fin increased, the heat transfer coefficient also increased as shown in Fig. 5. This finding aligns with fundamental principles of convective heat transfer in natural convection systems. In such systems, fluid motion is driven by buoyancy forces resulting from density differences caused by temperature gradients. When fins are closely spaced, the thermal boundary layers developing on adjacent fin surfaces quickly merge, effectively choking the inter-fin channel with slow-moving, warm fluid. This phenomenon, known as boundary layer interference, restricts the inflow of cooler fluid from the reservoir, thereby reducing the overall heat transfer coefficient.

As the spacing of fin is increased, more room is provided for these thermal boundary layers to develop independently before merging. This allows cooler water from the reservoir to penetrate deeper into the inter-fin channels before being heated. As a result, a greater portion of the fin surface is exposed to cooler water, enhancing the local temperature difference and thus the local heat transfer coefficient. Additionally, the wider spacing reduces the hydraulic resistance, allowing for stronger buoyancy-driven flows that further boost convective heat transfer.

The results also indicate that this increase in heat transfer coefficient does not necessarily lead to an overall decrease in thermal resistance. This is because thermal resistance is inversely proportional to the product of the heat transfer coefficient and the wetted surface area. While larger fin spacing improves the heat transfer coefficient, it simultaneously reduces the total wetted surface area available for heat transfer. For example, increasing the spacing of fin from 2.50 mm to 5.50 mm reduces the number of fins from 17 to 5, representing a significant 70% reduction in the number of fins and thus in the wetted surface area.

The results indicate that in this passive liquid cooling system, the loss in wetted surface area offsets any gains in heat transfer coefficient as the fin spacing increases. The temperature distribution plots shown in Fig. 5 of the presented paper support this conclusion. At a fin spacing of 3 mm, it is observed that the thermal boundary layers do not converge before leaving the top of the channels, indicating that this spacing is not ideal, as opposing boundary layers expand largely independently along the channel. On the other hand, a smaller fin spacing of 1 mm offers a different thermal profile. After a short period of thermal evolution, the boundary layers interact leading to the formation of mixed sections, where a significant rise in fluid temperature occurs along the channel. This indicates a more efficient use of the available surface area for heat transfer.

This work underscores a critical point in heat exchanger design: maximizing heat transfer is not simply about increasing the heat transfer coefficient. Instead, it requires a careful balance between enhancing convective heat transfer and providing sufficient surface area. In natural convection systems, where flow velocities are inherently low, surface area often plays a more dominant role. This explains why, despite the higher heat transfer coefficients, the larger spacing of fin 's resulted in higher thermal resistances.

The study offers valuable guidance for designing heat sinks in low-flow regimes typical of passive cooling systems. It suggests that within the constraints of the footprint is 40mm x 40mm, and the spacing of fin range of 2.50 to 5.50 mm was checked, The spacing between the fins should be as low as possible, because the increase in wetted surface area associated with the high packing density of the fins more than compensates for the decrease in convective heat transfer coefficient. These insights are crucial to optimizing thermal generator systems, where efficient cooling is necessary to maintain high temperature differences, enhancing power production and thermal efficiency.

The study exhibits that increasing the spacing of fin from 2.5 mm to 3.5 mm at hf=5mm results in a 25% boost of the heat transfer coefficient. The heat transfer coefficient reaches 45% enhancement when the spacing reaches 5.5 mm, while 4.5 mm produces a 37.5% enhancement, and 3.5 mm creates a 25% enhancement when compared to the initial 2.5 mm spacing. The heat transfer enhancement pattern for hf=10mm exhibits the same trends as it shows a 23.3% increase at 3.5 mm and then reaches a 40% increase at 4.5 mm while achieving a 53.3% increase at 5.5 mm when compared to the base spacing of 2.5mm. The results demonstrate that raising fin height assists heat removal, but the precise spacing of fin arrangement continues to influence heat transfer efficiency. The heat transfer coefficient increases by 27.3% when hf=15mm at 3.5 mm, but reaches 45.5% enhancement at 4.5 mm and 59.1% at 5.5 mm. The height of fins determines how significantly the spacing effects will benefit heat transfer operations because better fluid circulation and reduced boundary layer interference occur when spacing increases. When using hf=20mm as the fin height, the enhancements become even greater, resulting in 27.8% at 3.5 mm and 50% at 4.5 mm along with 66.7% at 5.5 mm. The expanded distance enables coolant fluid to penetrate effectively into the fins and produce improved convective heat transfer rates through hotspot reduction. When fins reach hf=25mm the heat transfer coefficient attains an 80% enhancement level at 5.5 mm spacing after increasing by 33.3% at 3.5 mm and 60% enhancement at 4.5 mm. Optimizing fin spacing proves to have significant importance in passive cooling systems because natural convection remains the primary heat transfer mechanism.

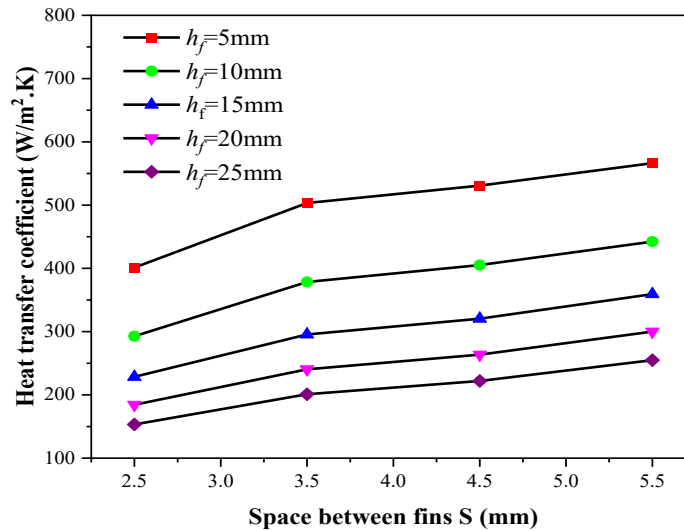


Fig. 5. Effect of space between fins on the heat transfer coefficient at different fin heights

3.2. Effect of fin height on the heat transfer coefficient

In this section of the study, four different fin heights were investigated: 5 mm, 10 mm, 15mm, 20 mm, and 25 mm on the heat transfer coefficient as shown in Fig. 6.

At a fin height of 5 mm, the fins only occupy a small portion of the cavity volume inside the manifold. This allows the incoming water flow from the inlet port to enter the manifold relatively unobstructed. The water is able to access the fin surfaces with minimal recirculation, resulting in higher velocities and wall shear stresses near the fin bases. Consequently, the heat transfer coefficient is relatively high for this short fin case.

As the fin height increases to 10 mm, the fins start to impede the inlet flow path causing some recirculation. However, the obstruction is still modest, and the increased surface area outweighs the small decrease in heat transfer coefficient. The net result is an improvement in overall heat transfer performance.

Continuing to increase the height to 15 mm and 20 mm, the fins occupy an even larger portion of the manifold cavity volume. This forces the inlet water to recirculate significantly before reaching the fins. While providing more surface area, the deteriorating flow conditions with increasing recirculation start to notably reduce the heat transfer coefficient due to the lowering of the wall shear stresses.

By 25 mm fin height, the fins extend across most of the manifold cavity height. The inlet flow is now severely constricted, resulting in substantial recirculation zones and stagnant flow regions near the fin bases. The heat transfer coefficient drops sharply as the wall shear stresses decrease with the declining flow velocities along the fins. Despite having the maximum surface area, the poor convective heat transfer negates potential benefits.

So in summary, increasing fin height from 5 mm initially improves overall heat transfer by providing more surface area without excessively disrupting the flow. However, once the fins become too tall (beyond ~20 mm for this configuration), the flow obstruction and recirculation patterns severely impede convective heat transfer by damping velocities and wall shear stresses. This causes the heat transfer coefficient to decrease sharply, resulting in a degradation of performance even though the surface area continues to increase.

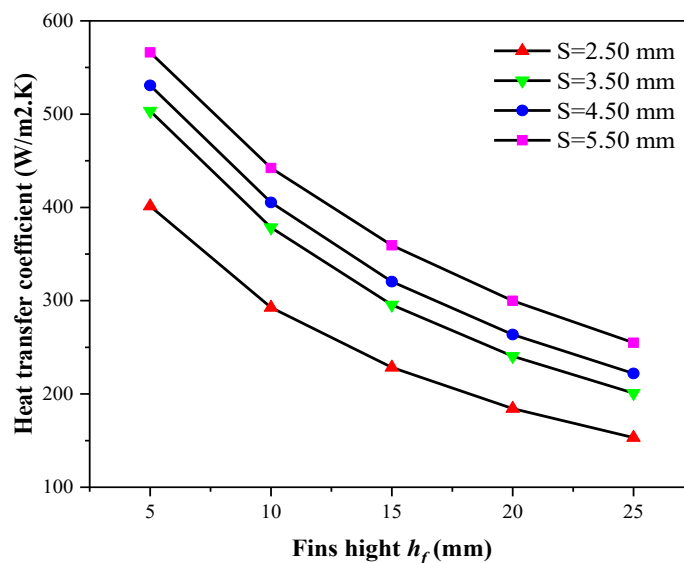


Fig. 6. Effect of fin height on the heat transfer coefficient at different fin spacings

3.3. Temperature and velocity contours

The effect of spacing of fins on the temperature distribution of the heat sink base was investigated through numerical simulations, with the fin height maintained at a constant value of 15 mm. Spacing of fins configurations analyzed were 2.50 mm, 3.50 mm, 4.50 mm, and 5.50 mm, as shown in Fig. 7.

The simulations revealed a significant impact of spacing of fin on the temperature profile of the heat sink base under natural convection conditions. Notably, the heat sink with the smallest spacing of fins 2.50 mm exhibited the lowest temperature on the base, indicating the most effective heat dissipation performance among the cases studied.

As the spacing of fins increased from 2.50 mm to 3.50 mm, a slight increase in the base temperature was observed. This trend continued with further increases in spacing of fins, where the heat sink with a 4.50 mm spacing of fins displayed higher base temperatures compared to the 3.50 mm configuration. The highest base temperatures were observed for the heat sink with a spacing of fins 5.50 mm, indicating the least effective heat dissipation among the scenarios examined.

The observed temperature distribution can be attributed to the interplay between spacing of fin and the resulting wetted surface area available for heat transfer. With a smaller spacing of fins 2.50 mm, the number of fins in the heat sink increases, leading to a larger total wetted surface area for heat dissipation. Despite the potential reduction in flow velocities due to increased flow resistance, the enhanced wetted surface area contributed to more effective heat transfer from the fins to the coolant, resulting in lower base temperatures.

Conversely, as the spacing of fins increased (3.50 mm, 4.50 mm, and 5.50 mm), the number of fins decreased, reducing the total wetted surface area available for heat transfer. Although the flow velocities may have increased slightly due to the reduced flow constriction, the reduction in surface area outweighed this effect, leading to higher temperatures on the heat sink base.

These results highlight the importance of optimizing spacing of fin in natural convection systems to strike a balance between maximizing wetted surface area for heat transfer and maintaining suitable flow characteristics. In the present study, the heat sink with a distance of fin 2.50 mm achieved optimal balance, resulting in the lowest base temperature and most effective heat dissipation performance under natural convection conditions.

In addition to the temperature distribution, the numerical simulations also provided insights into the flow velocity profiles for the different spacing of fin configurations under natural convection conditions. The velocity contours supported the previously established relationship between spacing of fin and flow velocities, wherein a decrease in spacing of fin led to a corresponding decrease in flow velocities.

For the heat sink with the smallest spacing of fins 2.50 mm, the velocity contours revealed the lowest flow velocities among the cases studied. As the spacing of fins increased to 3.50 mm, a slight increase in flow velocities was observed within the fin channels as shown in Fig. 8.

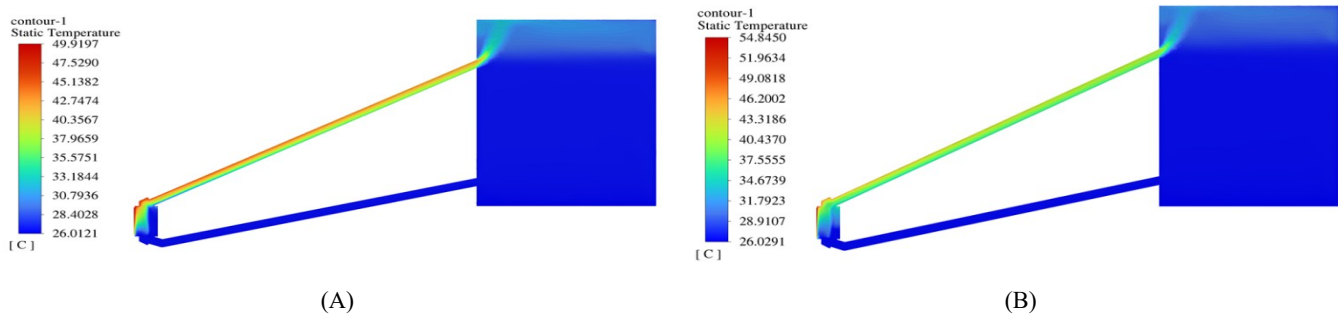
This trend of increasing flow velocities with increasing spacing of fin continued as the spacing of fins was further increased to 4.50 mm and 5.50 mm. The heat sink with the largest spacing of fin of 5.50 mm exhibited the highest flow velocities within the fin channels, indicating the least amount of flow constriction and resistance.

The observed velocity distribution can be attributed to the varying flow resistances imposed by the different spacing of fin configurations. With a smaller spacing of fins, such as 2.50 mm, the increased number of fins in the heat sink resulted in greater flow constriction and resistance, leading to lower flow velocities under the buoyancy-driven natural convection conditions.

Conversely, as the spacing of fins increased, the fins' number decreased, reducing the flow resistance and allowing for higher flow velocities within the fin channels. The heat sink with the largest spacing of fin of 5.50 mm offered the least amount of flow constriction, resulting in the highest flow velocities observed in the simulations.

These velocity results align with the previously discussed temperature distribution findings, where the heat sink with the smallest spacing of the fins of 2.50 mm exhibited the lowest base temperatures. Despite the lower flow velocities associated with the smaller spacing of fin, the raised wetted surface area provided by the higher fins' number contributed to more effective heat dissipation, leading to the observed temperature reduction.

The velocity contours underscore the intricate interplay between the spacing of fins, flow resistance, and heat transfer performance in natural convection systems, emphasizing the need for careful optimization to achieve the desired balance between these factors.



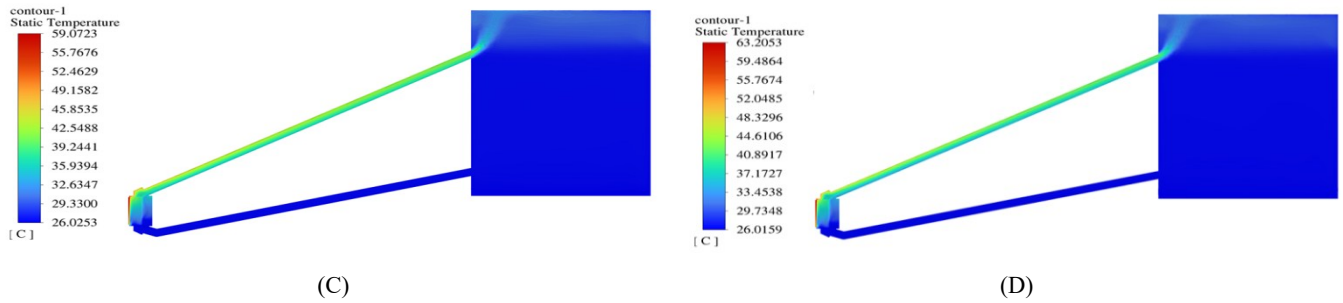


Fig. 7. Effect of spacing of fins on the temperature distribution with a fin height of 15 mm and spacing configurations at (A: 2.50, B: 3.50, C: 4.50, and D: 5.50) mm

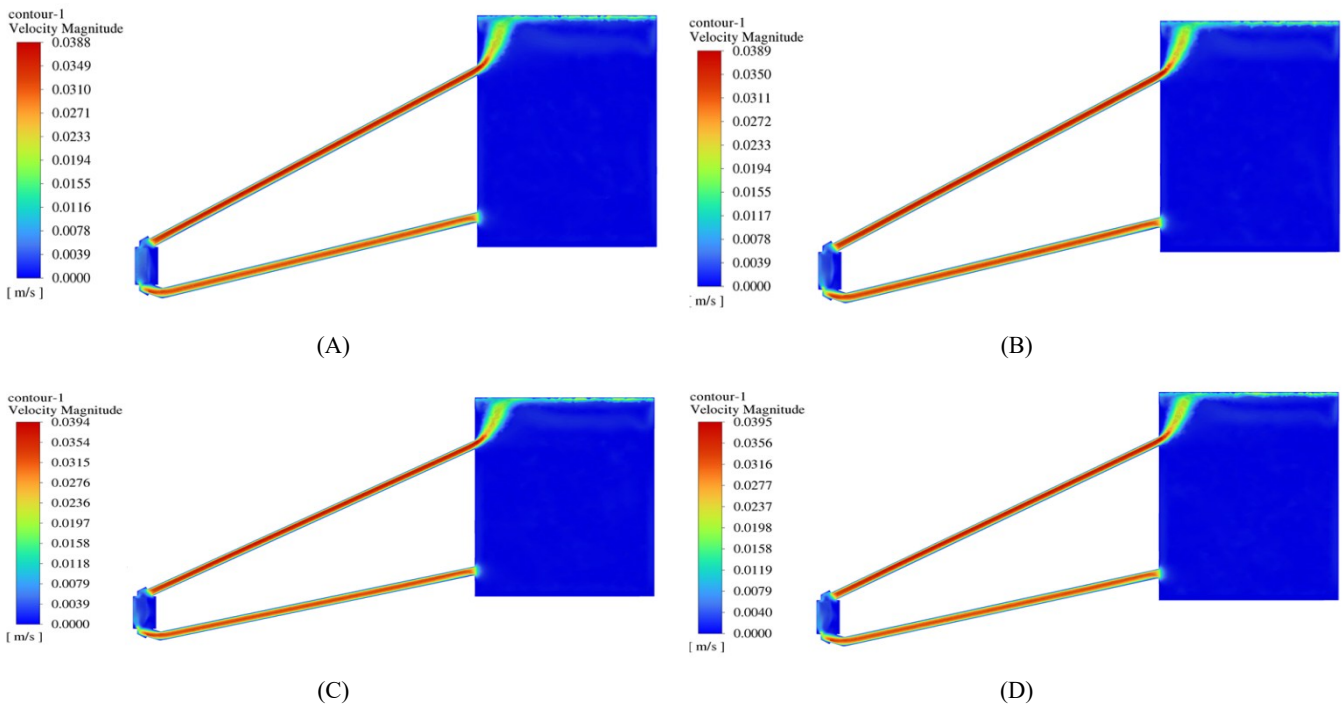


Fig. 8. Effect of spacing of fins on the velocity distribution with a fin height of 15 mm and spacing configurations at (A: 2.50, B: 3.50, C: 4.50, and D: 5.50) mm

3.4. Effect of nanofluid on heat transfer coefficient

The intent of this study was to test the enhancement of a passive liquid cooling system for thermoelectric generators (TEGs) through the use of nanofluids. Indeed, their heat sink water was replaced by Al_2O_3 -water and CuO -water nanofluids with different nanoparticle concentrations (1 to 4%). A heat sink geometry optimized for the given conditions, with spacing of fin of 2.50 mm and a fin height of 15 mm, was used to perform computational fluid dynamics (CFD) simulations. Comparatively, this configuration resulted in better heat transfer and a larger temperature reduction in the heat sink than the previously tested geometries.

The heat transfer performance was greatly improved when nanofluids were introduced into the cooling system. Fig. 9 shows that both Al_2O_3 -water and CuO -water nanofluids possess higher heat transfer coefficients than those of pure water. The higher thermal conductivity of the nanofluids is due to the fact that the nanofluid contains highly conductive nanoparticles to disperse, which is the main reason for this enhancement.

Interestingly, Al_2O_3 -water nanofluid was found to have a higher heat transfer coefficient, based on the simulations. In line with expectations, it turns out that the thermal conductivity of Al_2O_3 nanoparticles exceeds that of CuO nanoparticles. This substantial difference in thermal conductivity is the main reason to explain Al_2O_3 -water nanofluid's superior performance.

The network structure that develops when nanoparticles are dispersed in a fluid allows heat conduction. Al_2O_3 nanoparticles have higher thermal conductivity and are able to form more heat conducting networks in the fluid than the base fluid, resulting in higher heat transfer. Since Al_2O_3 nanoparticles have high thermal conductivity, heat is quickly removed from the heat sink surface, traveling through the nanoparticle network into the bulk fluid. The Al_2O_3 -water Nano fluid exhibits an efficient heat transfer mechanism that greatly enhances the overall heat transfer coefficient.

The heat transfer coefficient of both nanofluids increases with increasing concentration of nanoparticles. The trend persisted across the simulations. The heat transfer capability is improved with the addition of more particles to conduct the heat and interact with the fluid. This effect is more pronounced in the Al_2O_3 -water Nano fluid, likely due to the higher thermal conductivity of Al_2O_3 nanoparticles.

It's worth noting that while this study focused on heat transfer coefficient, the ultimate goal is to reduce the thermal resistance of the heat sink, which also depends on the surface area. The choice of 2.50 mm fin spacing and 15 mm fin height represents a balance between maximizing surface area and maintaining adequate flow between the fins. This is in line with previous findings that decreasing the fin spacing (down to fabrication limits) generally improves heat sink performance, despite the accompanying decrease in the convective heat transfer coefficient.

In conclusion, this computational study demonstrates that replacing water with nanofluids in the passive cooling system for TEGs can enhance heat transfer performance. These findings suggest that Nano fluids, especially Al_2O_3 -water, could be a promising avenue for improving the efficiency of TEG cooling systems, potentially leading to higher power output and thermal efficiency.

In this study, the base condition of water exhibits a heat transfer coefficient at $247 \text{ W/m}^2\text{K}$. The heat transfer coefficient reached $258 \text{ W/m}^2\text{K}$ when the 1% concentration was used causing a 5.31% enhancement. An increase in heat transfer coefficient to $270 \text{ W/m}^2\text{K}$ happens when the Nano fluid concentration reaches 2% which leads to an enhancement of 10.20%. The heat transfer coefficient of $285 \text{ W/m}^2\text{K}$ corresponds to a 16.33% enhancement when the Nano fluid concentration reaches 3%. Furthermore, the highest improvement of 20.41% leads to a heat transfer coefficient of $295 \text{ W/m}^2\text{K}$ at 4% concentration.

In the case of CuO nanofluid, the heat transfer coefficient rises to $250 \text{ W/m}^2\text{K}$ at 1% concentration, enabling an enhancement of 2.04%. The nanofluid achieves its highest heat enhancement value of 4.90% at a 2% concentration, which produces a value of $257 \text{ W/m}^2\text{K}$. The overall increase in the heat transfer coefficient to $265 \text{ W/m}^2\text{K}$ occurs at a 3% concentration, resulting in an 8.16% improvement. The heat transfer coefficient reaches $272 \text{ W/m}^2\text{K}$ after increasing the concentration to 4% producing an 11.02% enhancement.

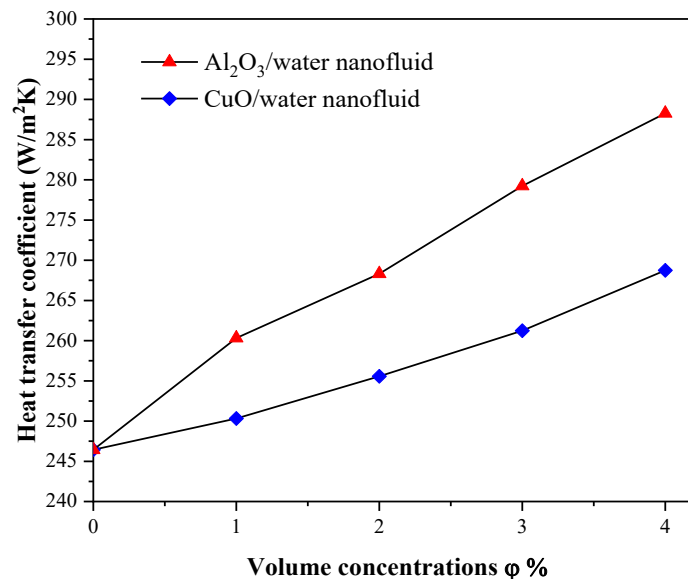


Fig. 9. Effect of Nano fluids on the heat transfer coefficient at a fin height of 15 mm and a fin distance of 2.50 mm

3.5. Thermoelectric power generation performance

The performance of the TEG system was evaluated under high heat flux conditions, where the hot side of the system experiences a high heat flux of up to $75,000 \text{ W/m}^2$. In order to handle this very high thermal input on the cold side, a finned heat sink was used to keep the cold side at a lower temperature. Fins on the heat sink were 15 mm high and spaced 2.50 mm apart, resulting in a significant surface area for adequate thermal dissipation.

The performance of the heat sink has been significantly improved by using Nano-liquid as the coolant. This advanced cooling solution provided excellent thermal performance and better convection heat transfer properties than conventional chillers. As a result, the heat sink effectively reduced the cold side temperature to $39 \text{ }^\circ\text{C}$, despite the high heat flux on the hot side. This substantial temperature reduction is critical for maintaining the high temperature gradient across the TEG, which is essential for efficient thermoelectric power generation.

Fig. 10 shows the temperature contours obtained from the simulation, providing visual evidence of the thermal management's effectiveness. These contours clearly depict the temperature distribution across the TEG system, showing a stark contrast between the hot and cold sides. This pronounced temperature gradient is the driving force behind the thermoelectric effect, where the movement of charge carriers (electrons or holes) from the hot side to the cold side generates an electric potential difference.

Fig. 11 shows the voltage contours derived from the simulation, further corroborating the TEG's power generation capability. These contours illustrate the spatial distribution of electrical potential across the TEG module, indicating regions of higher and lower voltages (1.07 to 11.07 mV). The presence of these voltage gradients confirms that the Seebeck effect is effectively converting the temperature difference into electrical energy.

Similarly, the current density contours shown in Fig. 12 provide insight into the flow of electric charges within the TEG. These contours show the magnitude and direction of current flow, which is a direct result of the voltage difference created by the temperature gradient. Higher current densities signify more substantial charge carrier movement, translating to greater power output.

In summary, our TEG system, when exposed to a high heat flow of $75,000 \text{ W/m}^2$, successfully generated electrical power. The cold side temperature of $39 \text{ }^\circ\text{C}$ was maintained, which was attributed to the effective thermal management supplied by the finned heat sink cooled by the

nanofluid. Voltage and current density contours have also shown that the resulting high temperature gradient induced a strong thermoelectric effect. We see our TEG results as enhancing the potential of our system in high-flow applications, where large amounts of waste heat can be transformed into useful electrical energy.

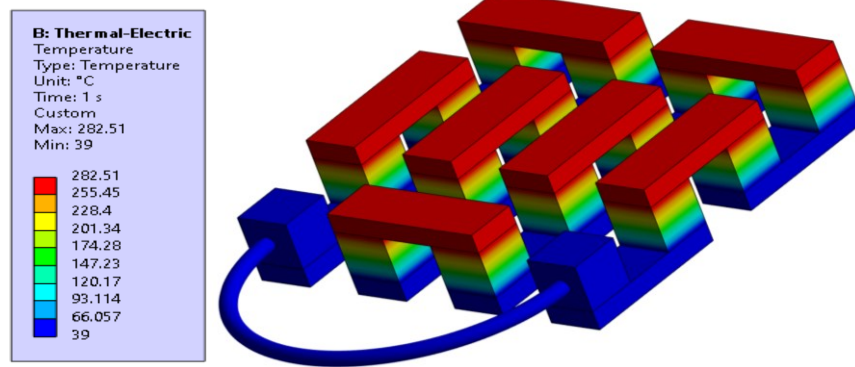


Fig. 10. Simulated temperature distribution in the TEG configuration

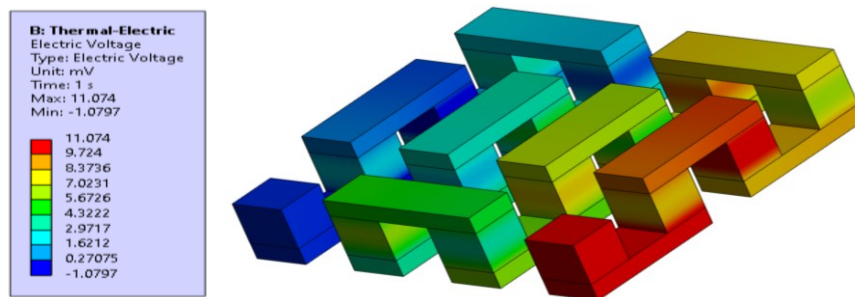


Fig. 11. Simulated electric voltage distribution in the TEG configuration

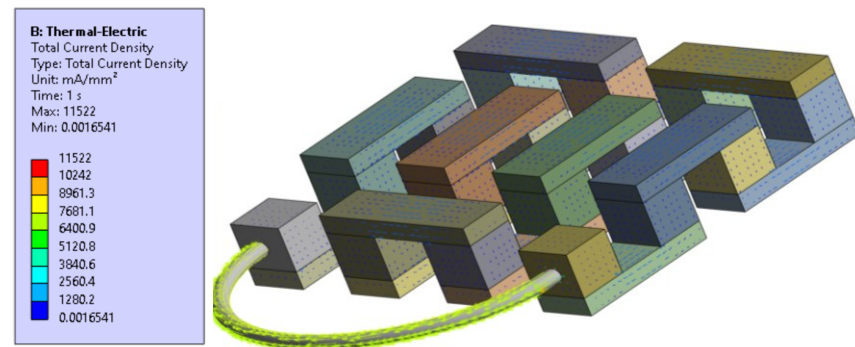


Fig. 12. Simulated current density vector in the TEG configuration

4. Conclusion

This research has thoroughly addressed the challenge of optimizing thermoelectric generators (TEGs) to convert waste heat into electricity by improving their thermal performance. Through numerical investigations, the study examined the effects of geometric configurations and advanced cooling fluids on TEG efficiency and reliability. The findings revealed that the optimal spacing of fins for heat sinks is 2.50 mm, as wider spacing increases the heat transfer coefficient but leads to higher temperatures due to the loss of wetted surface area. Fin heights between 5 mm and 25 mm were found to improve heat dissipation by increasing wet surface area, despite lowering the local convective heat transfer coefficient. Regarding cooling, (Al₂O₃ and CuO) water Nano fluids outperformed pure water, with Al₂O₃-water reducing heat sink temperature by 17% at a 4% concentration, while CuO-water achieved a 13% reduction. Increasing Al₂O₃-water nanoparticle concentration from 1% to 4% provided an additional 8°C temperature drop, highlighting the benefits of higher concentrations. During high-flux testing, the optimized TEG system, featuring a 15 mm fin height and 2.50 mm spacing of fins, maintained a cold side temperature of 39 °C under a heat flux of 75,000 W/m² when cooled by nanofluids. This underscores the effectiveness of combining geometric optimization and advanced nanofluids in managing extreme thermal loads. Simulations visually confirmed the system's ability to maintain critical temperature gradients necessary for substantial TEG power generation. Overall, this research demonstrates that integrating geometric optimization with advanced Nano fluids can significantly enhance the thermal performance of TEG systems, offering valuable guidelines for designing more efficient and reliable TEGs and contributing to improved waste heat recovery and energy conversion technologies, supporting broader energy efficiency and sustainability initiatives.

Acknowledgment

I would like to thank the Department of Energy Conversion, Mechanical Engineering College, Iran University of Science and Technology, for supporting the project requirements.

References

- [1] H. Ma, J. Cao, and Q. Sheng, "A Review on Heat Transfer Performances of Thermosiphons Using Nanofluids," presented at the E3S Web of Conferences, EDP Sciences, 2024, p. 01001. [Online]. Available: <https://doi.org/10.1051/e3sconf/202456001001>
- [2] M. A. Nadim, I. A. Zakaria, B. S. B. Singh, W. A. N. W. Mohamed, and R. Bahsan, "Al₂O₃ and SiO₂ Nanofluids Performance in Thermoelectric Generator," *J. Adv. Res. Fluid Mech. Therm. Sci.*, vol. 107, no. 1, pp. 45–57, 2023, doi: <https://doi.org/10.37934/arfmts.107.1.4557>.
- [3] M. A. Abdelkareem et al., "Prospects of thermoelectric generators with nanofluid," *Therm. Sci. Eng. Prog.*, vol. 29, p. 101207, 2022, doi: <https://doi.org/10.1016/j.tsep.2022.101207>.
- [4] Y. Köysal, Y. Yakut, S. Özbektaş, H. Bülbül, T. Atalay, and F. Şahin, "Evaluation of energy efficiency of thermoelectric energy generator system with heat pipes, solar tracker, Fresnel lens and nano-particle fluids," *Appl. Therm. Eng.*, vol. 246, p. 123027, 2024, doi: <https://doi.org/10.1016/j.applthermaleng.2024.123027>.
- [5] C. F. Ramos-Castañeda, M. A. Olivares-Robles, A. E. Olivares-Hernandez, and L. Hernandez-Gonzalez, "Performance of a Nanofluid-Cooled Segmented Thermoelectric Generator: Hollow/Filled Leg Structures and Segmentation Effects," *Processes*, vol. 11, no. 6, p. 1728, 2023, doi: <https://doi.org/10.3390/pr11061728>.
- [6] J. Xing, Z. Wu, H. Xie, Y. Wang, Y. Li, and J. Mao, "Performance of thermoelectric generator with graphene nanofluid cooling," *Chin. Phys. B*, vol. 26, no. 10, p. 104401, 2017, doi: [10.1088/1674-1056/26/10/104401](https://doi.org/10.1088/1674-1056/26/10/104401).
- [7] R. Seok-Ho, S. Dong-Ryun, and L. Taek-Kyu, "Development of Nanofluidic Thermosyphon Heat Sink," *Korean J. Air-Cond. Refrig. Eng.*, vol. 18, no. 10, pp. 826–834, 2006, doi: <https://koreascience.kr/article/JAKO200634742895935.page>.
- [8] S. Y. Qin et al., "Experimental study on the thermal characteristics of a 3D thermosyphon heat sink," *Appl. Therm. Eng.*, vol. 225, p. 120193, 2023, doi: <https://doi.org/10.1016/j.applthermaleng.2023.120193>.
- [9] K. S. Garud et al., "Thermal–electrical–structural performances of hot heat exchanger with different internal fins of thermoelectric generator for low power generation application," *J. Therm. Anal. Calorim.*, vol. 143, no. 1, pp. 387–419, Jan. 2021, doi: [10.1007/s10973-020-09553-7](https://doi.org/10.1007/s10973-020-09553-7).
- [10] A. H. D. K. Rasangika, M. S. Nasif, and R. Al-Waked, "Numerical investigation on the thermal performance of perforated and non-perforated twisted fins at different twisting angles," *Results Eng.*, p. 102332, 2024, doi: <https://doi.org/10.1016/j.rineng.2024.102332>.
- [11] T. Ghouchi, M. Pourfallah, and M. Gholinia, "The thermal and hydrodynamic analysis in a heat sink with different configurations of shark scales-based fins," *Appl. Therm. Eng.*, p. 123492, 2024, doi: <https://doi.org/10.1016/j.applthermaleng.2024.123492>.
- [12] J. Park, S. Hong, K. Kwak, and J.-H. Jeong, "Numerical Investigation of Performance Enhancement for Thermoelectric Generator System Optimization of HX Fin Shape," *Int. J. Energy Res.*, vol. 2024, no. 1, p. 6628332, 2024, doi: <https://doi.org/10.1155/2024/6628332>.
- [13] H. Ramezani, J. Bakhshi, M. Ghasemian, and M. Sheikholeslami, "A numerical investigation of the effect of a heat sink with sinusoidal fins on the performance of high-concentrated solar cells," *Appl. Therm. Eng.*, vol. 236, p. 121746, 2024, doi: <https://doi.org/10.1016/j.applthermaleng.2023.121746>.
- [14] R. Quan, J. Wang, W. Liang, X. Li, and Y. Chang, "Numerical investigation of a thermoelectric generator system with embedded sickle-shaped fins," *Appl. Therm. Eng.*, vol. 236, p. 121741, 2024, doi: <https://doi.org/10.1016/j.applthermaleng.2023.121741>.
- [15] C. Veer, K. Kansara, and S. Singh, "Numerical Study on the Performance Evaluation and Thermal Management of Automotive Exhaust Thermoelectric Generator using Pin fins," 2023, doi: <https://doi.org/10.21203/rs.3.rs-3583330/v5>.
- [16] Z. Hu, F. de León, R. Wang, and Y. Li, "Effects of Installing Different Types of Cooling Fins on the Cold Side of a Thermoelectric Power Generation Device on the Thermal Efficiency and Exergy Efficiency of Power Cable Surface Waste Heat Recovery," *Micromachines*, vol. 14, no. 8, p. 1591, 2023, doi: <https://doi.org/10.3390/mi14081591>.
- [17] M. R. Salim, A. Abas, K. H. Lim, and M. N. Abdullah, "Performance of power dissipation on semiconductor module for different configuration of heat SINK with thermal pad," *Int. J. Therm. Sci.*, vol. 201, p. 109045, 2024, doi: <https://doi.org/10.1016/j.ijthermalsci.2024.109045>.
- [18] M. Chen, L. A. Rosendahl, and T. Condra, "A three-dimensional numerical model of thermoelectric generators in fluid power systems," *Int. J. Heat Mass Transf.*, vol. 54, no. 1–3, pp. 345–355, 2011, doi: <https://doi.org/10.1016/j.ijheatmasstransfer.2010.08.024>.
- [19] B. C. Pak and Y. I. Cho, "Hydro Dynamic and Heat Transfer Study of Dispersed Fluids with Submicron Metallic Oxide Particles," *Exp. Heat Transf.*, vol. 11, no. 2, pp. 151–170, Apr. 1998, doi: [10.1080/08916159808946559](https://doi.org/10.1080/08916159808946559).
- [20] R. Ben-Mansour and M. A. Habib, "Use of Nanofluids for Improved Natural Cooling of Discretely Heated Cavities," *Adv. Mech. Eng.*, vol. 5, p. 383267, Jan. 2013, doi: [10.1155/2013/383267](https://doi.org/10.1155/2013/383267).
- [21] O. A. Alawi et al., "Heat transfer and hydrodynamic properties using different metal-oxide nanostructures in horizontal concentric annular tube: An optimization study," *Nanomaterials*, vol. 11, no. 8, p. 1979, 2021, doi: <https://doi.org/10.3390/nano11081979>.
- [22] S. H. Mullick, D. DasGupta, and P. K. Kundu, "Numerical investigation on natural convection inside closed cavity to create thermally active region with periodic heating/cooling," *J. Therm. Anal. Calorim.*, vol. 147, no. 23, pp. 13861–13878, Dec. 2022, doi: [10.1007/s10973-022-11688-8](https://doi.org/10.1007/s10973-022-11688-8).
- [23] D. P. Kulkarni, D. K. Das, and S. L. Patil, "Effect of temperature on rheological properties of copper oxide nanoparticles dispersed in propylene glycol and water mixture," *J. Nanosci. Nanotechnol.*, vol. 7, no. 7, pp. 2318–2322, 2007, doi: <https://doi.org/10.1166/jnn.2007.437>.
- [24] M. K. Moraveji and R. M. Ardehali, "CFD modeling (comparing single and two-phase approaches) on thermal performance of Al₂O₃/water nanofluid in mini-channel heat sink," *Int. Commun. Heat Mass Transf.*, vol. 44, pp. 157–164, 2013, doi: <https://doi.org/10.1016/j.icheatmasstransfer.2013.02.012>.
- [25] V. Bianco, F. Chiacchio, O. Manca, and S. Nardini, "Numerical investigation of nanofluids forced convection in circular tubes," *Appl. Therm. Eng.*, vol. 29, no. 17–18, pp. 3632–3642, 2009, doi: <https://doi.org/10.1016/j.applthermaleng.2009.06.019>.

- [26] H. A. Kazem, M. T. Chaichan, and A. H. A. Al-Waeli, "Effect of CuO-water-ethylene glycol nanofluids on the performance of photovoltaic/thermal energy system: an experimental study," *Energy Sources Part Recovery Util. Environ. Eff.*, vol. 44, no. 2, pp. 3673–3691, Jun. 2022, doi: 10.1080/15567036.2022.2070305.
- [27] O. T. Olakoyejo, E. Adeyemi, O. O. Adewumi, S. M. Abolarin, I. A. Fetuga, and A. O. Adelaja, "Numerical Investigation of Two-Phase Thermal-Hydraulic Characteristics and Entropy Generation of Water-Based Al₂O₃-Cu Hybrid Nanofluids in Microchannel Heat Sink," *ITEGAM-JETIA*, vol. 11, no. 51, 2025, doi: <https://doi.org/10.5935/jetia.v11i51.1487>.
- [28] S. A. Hussein and S. J. Shbailat, "Experimental and numerical study of forced convective heat transfer in a horizontal circular pipe with varying angles ribs," *Int. J. Adv. Technol. Eng. Explor.*, vol. 9, no. 93, p. 1246, 2022, doi: <http://dx.doi.org/10.19101/IJATEE.2021.875728>.
- [29] M. Corcione, "Empirical correlating equations for predicting the effective thermal conductivity and dynamic viscosity of nanofluids," *Energy Convers. Manag.*, vol. 52, no. 1, pp. 789–793, 2011, doi: <https://doi.org/10.1016/j.enconman.2010.06.072>.
- [30] M. Salari, M. R. Assari, A. Ghafouri, and N. Pourmahmoud, "Empirical correlations for thermal conductivity and dynamic viscosity of MgO-EG," *J. Braz. Soc. Mech. Sci. Eng.*, vol. 43, no. 2, p. 111, Feb. 2021, doi: 10.1007/s40430-020-02773-w.